Spontaneous Oxidation of Organic Matter and Ammonium Uptake from Manure Wastewater by Redox-Active Materials

Rui Wang[1], Anneke Moeller[1], Hanyu Tang[2], Paulo Falco Cobra[3], Mohan Qin[2], Song Jin[1]*

[1] Department of Chemistry, University of Wisconsin-Madison, Madison, Wisconsin 53706, USA.

[2] Department of Civil and Environmental Engineering, University of Wisconsin-Madison, Madison, Wisconsin 53706, USA.

[3] Department of Biochemistry, University of Wisconsin-Madison, Wisconsin, Wisconsin 53706, USA.

*E-mail: jin@chem.wisc.edu;

Abstract

Spontaneous NH_4^+ uptake using solid-state redox-active materials, driven by the oxidation of organic matter in manure wastewater, provides a sustainable and energy-friendly method for nutrient recovery. However, the mechanism of electron transfer and accompanying ion transport are poorly understood. Here, we investigated the electron transfer pathway and NH_4^+ uptake mechanism by analyzing the composition changes in manure wastewater via NMR and the corresponding electrochemical results. We found that the spontaneous NH_4^+ uptake involves a direct electron transfer process without redox mediators, with the co-occurrence of ion intercalation and adsorption. Based on the elucidated mechanisms, a core-shell Prussian blue analogue redox material with improved stability in manure wastewater and enhanced NH_4^+ recovery compared to previously reported electrode materials was developed. Such a fundamental understanding of the oxidation of organic compounds and spontaneous NH_4^+ uptake by redox-active materials can guide the design of redox materials for effective resource recovery and environmental applications.

Battery electrode materials, essentially solid-state redox-active materials, have played a critical role in the ongoing transformation of renewable energy technologies by converting and storing electrical energy into electrochemical energy, enabling mobile electronics, electrified

transportation, and grid-scale energy storage.[1-5] Battery materials can also temporarily store electrons and ions and redirect them to pair with different electrochemical or chemical processes.[6-14] When the electrochemical potential of redox-active materials is sufficiently high, they can spontaneously react with the organic molecules in the electrolyte. For battery electrode materials, such spontaneous reaction between organic electrolytes and anodes is not desirable and often kinetically inhibited by the formation of the solid-electrolyte interphase (SEI).[15, 16] On the other hand, traditional chemical synthesis has utilized various redox-active materials as heterogeneous oxidants in aqueous or organic solutions.[17] For example, nickel peroxide (NiO_2) can oxidize alcohols, amines, Schiff's bases, and other organic compounds with high yields (> 80 %) and high selectivity at room or evaluated temperatures.[18-20] Beyond simple redox systems with pure reactants, redox-active natural minerals with relatively high electrochemical potentials can also oxidize organic matter from natural water and remove organic contaminants from wastewater.[21] For example, Earth-abundant manganese oxides (MnO_2) have been explored to oxidize humic substances[22] and other organic compounds like phenols and organic acids in soils or wastewater.[23-27] Despite these studies on the use of solid-state redox-active materials for the oxidation of organic compounds in organic synthesis[27] and contaminant removal,[25] the reduction mechanisms of redox-active materials and guidelines for developing more effective redox-active materials remain unclear.

It is often overlooked but worth noting that the electron transfer between redox-active materials and organic compounds is always accompanied by ion transport. Transport of protons, which are always available in aqueous solutions, is usually coupled with electron transfer to maintain the charge balance of redox materials, such as from NiO_2 or NiOOH to $Ni(OH)_2$,[28, 29] or the reductive dissolution of MnO_2 to Mn^{2+}.[24] Redox-active materials that can selectively intercalate ions also provide opportunities for resource recovery.[30-35] Recently, our group developed an efficient electrochemical approach for ammonium (NH_4^+) recovery and co-production of chemicals from manure wastewater using a Prussian blue analogue (PBA) redox reservoir (RR) material, potassium nickel hexacyanoferrate (KNiHCF).[36] An unusual aspect of this electrochemical process is that the KNiHCF electrode could spontaneously oxidize organic compounds present in manure wastewater and uptake nutrient ions (NH_4^+ and K^+) with a high selectivity. The thermodynamic driving force of spontaneous NH_4^+ uptake is believed to be the electrochemical potential difference between the redox potentials of the KNiHCF electrode and

the organic compounds. However, the electron transfer mechanism in the complicated manure wastewater was unclear, especially given the numerous metabolites and microorganisms present in manure wastewater that may serve as chemical or biological mediators.[37, 38] Understanding the spontaneous oxidation of organic compounds in manure wastewater and elucidating possible electron transfer pathways to the KNiHCF electrode would provide new insights into developing more effective redox materials for resource recovery and organic removal.

In this study, we investigate the electron transfer pathway from organic compounds in manure wastewater to redox-active materials and the NH_4^+ uptake mechanism using KNiHCF as the model electrode (Fig. 1a). By examining the effect of microorganisms and the compositions of dissolved organic compounds by nuclear magnetic resonance (NMR), we identify direct electron transfer (Fig. 1b), as opposed to mediated electron transfer (Fig. 1c), in such an oxidation process on the redox electrode.[30] The concentration changes of organic compounds and corresponding electrochemical results during NH_4^+ recovery reveal the co-occurrence of the ion intercalation and adsorption on the redox-active electrode in manure wastewater (Fig. 1d). Based on the elucidated mechanism, we further design CuHCF@KNiHCF core-shell redox material with higher redox potential and a similar interface that shows improved performance in NH_4^+ uptake and oxidation of organic compounds than the model KNiHCF material. These insights into the electron transfer pathways and material design principles are crucial for developing more efficient and selective redox systems for resource recovery and environmental applications.

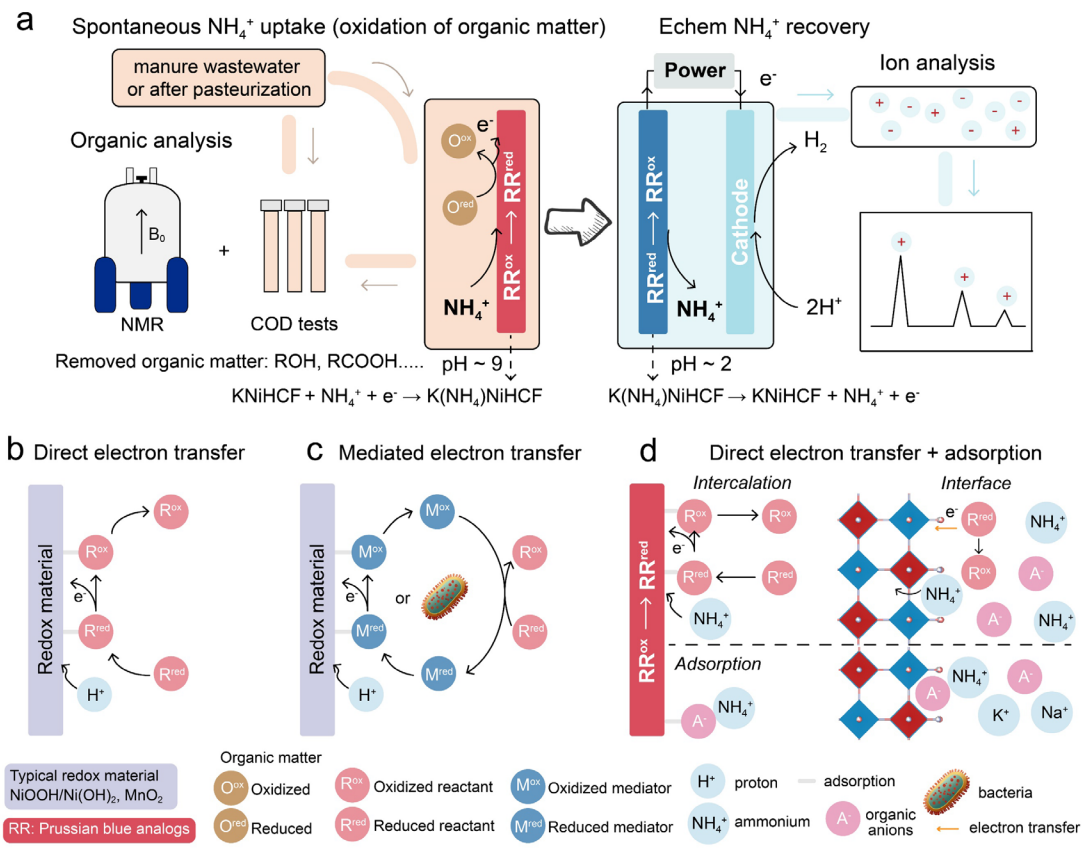

Figure 1. Studies on the electron transfer from organic matter to redox-active KiNiHCF material and the accompanied ion transport. (a) Schematic illustration of spontaneous oxidation of organic matter and electrochemical NH_4^+ recovery from manure wastewater and the NMR and ionic chromatography analysis on the organic compounds and pertinent ions in manure wastewater and recovered solutions. Illustration of the processes of: (b) direct electron transfer from organic matter to redox-active materials vs. (c) mediated electron transfer through redox mediators or microorganisms to redox-active materials. Here, proton-coupled electron transfer is shown as an example; (d) furthermore, direct electron transfer from organic matter to redox-active materials accompanied by selective ion intercalation vs. ion adsorption. NH_4^+ is shown in (d) as an example of selectively intercalated cations.

We first studied the effect of microorganisms present in manure wastewater to identify whether electrons transfer from organic matter to redox-active materials goes through direct electron transfer (Fig. 1b) or mediated electron transfer (Fig. 1c). The difference between the two pathways is whether chemical or biological mediators participated in the redox process.[39] KNiHCF with good stability was used as the model redox material with a specific capacity of 186 C g^{-1} (see

Materials and Methods in the SI). We conducted the spontaneous ammonia uptake in manure wastewater with a pH of 9. Given that the *pK*a of "$NH_4^+ \leftrightharpoons H^+ + NH_3$" is 9.2, 39 % of ammonia is present as NH_3 in manure wastewater, and the other is as NH_4^+. Considering the chemical equilibrium and proton generation during the oxidation of organic matter, the continuous conversion from NH_3 and protons to NH_4^+ occurs during the spontaneous NH_4^+ uptake. To kill bacteria/pathogens or inactivate bio-mediators in manure wastewater, we pasteurized manure wastewater under N_2 at 100 ºC for 24 hours (Fig. S1) or froze manure wastewater at ‑80 ºC for three days (see Methods). The cation concentrations in manure wastewater did not change much after pasteurization treatment (Fig. 2a), except the decrease of NH_4^+ concentration from 497 ± 23 mM to 393 ± 5 mM, which might result from the NH_3 evaporation. We conducted three parallel NH_4^+ recovery runs (noted as run 1, run 2, and run 3) in manure wastewater before and after pasteurization using the same KNiHCF electrode, which included spontaneous NH_4^+ uptake in (treated) manure wastewater and then electrochemical NH_4^+ recovery paired with hydrogen evolution reaction in 0.1 M Li_2SO_4 solution (pH~2) (see Methods).[36] The NH_4^+ removal of ~67 % and nutrient selectivity of over 90 % in pasteurized manure wastewater were similar to those in unpasteurized manure wastewater (Fig. 2b). The chemical oxygen demand (COD) removal of 28.1 ± 1.9 % in pasteurized manure wastewater was similar to that in manure wastewater (30.9 ± 1.6 %) (Fig. 2c). The NH_4^+ removal and COD removal in manure wastewater that has gone through freezing treatment also did not show obvious changes compared to untreated manure wastewater (Fig. S2). Therefore, unlike microbial fuel cells, where microorganisms play an essential role in oxidizing organic molecules,[40, 41] the spontaneous oxidation of organic matter and NH_4^+ uptake using redox-active materials can occur in manure wastewater without active microorganisms.

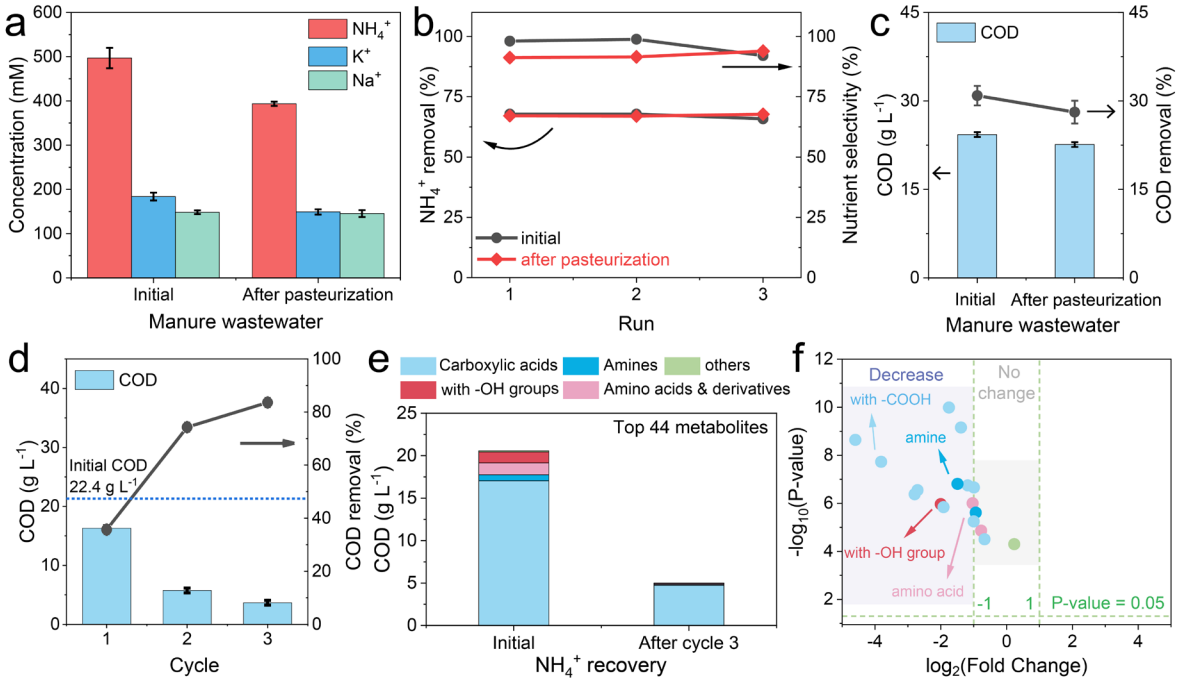

Figure 2. Effect of microorganisms on the spontaneous oxidation of organic matter and NH_4^+ uptake by KNiHCF electrode and the compositional changes of organic compounds in manure wastewater after oxidation. (a) Concentration changes of NH_4^+, K^+, and Na^+ in manure wastewater before and after pasteurization treatment. (b) The NH_4^+ removal and nutrient selectivity by the KNiHCF electrode and (c) COD removal in manure wastewater through the electrochemical NH_4^+ recovery process from the manure wastewater before and after pasteurization treatment. (d) Measured COD and COD removal over a three-cycle NH_4^+ recovery process in manure wastewater and (e) corresponding calculated COD based on the NMR analysis of the organic metabolite compounds in manure wastewater. (f) Volcano plot of various metabolites in manure wastewater based on the NMR analyses before and after NH_4^+ recovery. Each dot represents one metabolite. Dots above the horizontal green dash line represent metabolites with $p < 0.05$ ($-\log10(\text{p-value}) > 1.3$) while those below the line represent those with $p > 0.05$. Dots in the light purple area represent metabolites that show significant concentration changes ($|\log_2 FC| \geqslant 1$). Dots in the grey area represent metabolites without significant concentration changes ($|\log_2 FC| < 1$).

We conducted a comprehensive NMR analysis of the soluble organic compounds (metabolites) in manure wastewater (see Methods) to explore possible chemical mediators and

electron donors. We identified the top 44 metabolites in manure wastewater and classified them into five categories (Table S1): carboxylic acids, amines, amino acids and derivatives, metabolites with -OH groups, and others. The calculated COD based on the NMR results of all metabolites (20.6 g L^{-1}) was remarkably close to the measured COD (22.4 g L^{-1}) (see details of calculation in Note S1 and results in Table S2), partially confirming the reliability of NMR analysis. The top 44 metabolites, however, did not contain possible chemical mediators with reversible redox functional groups (e.g., C=O or C=N bonds),[42-44] suggesting that the electron transfer process during the oxidation of organic matter may not be a mediated process.

We then conducted a three-cycle NH_4^+ uptake and recovery from manure wastewater and analyzed its composition changes. Cycles 1 and 2 removed similar absolute amount and percentage of the initial COD, but cycle 3 removed much less, reaching an accumulated COD removal of 83% (Fig. 2d). One might expect a more equal absolute amount of COD removal each cycle and a linear progression of the accumulated percentage COD removal. During cycle 3, the redox-active electrode could not effectively oxidize the remaining organic species after two oxidation cycles. The slight change in COD removal from cycles 1 to 2 might result from the volume reduction of manure wastewater due to sampling for COD analysis (see Methods).

Nearly all peaks in the NMR spectra of manure wastewater after 3-cycle NH_4^+ uptake decreased, and some peaks disappeared (Fig. S3). Detailed comparison of the concentrations of metabolites before and after showed that nearly all amino acids and derivatives and metabolites with -OH groups, most amines, and some carboxylic acids were removed (Table S3). The calculated COD removal based on NMR results before and after NH_4^+ recovery was ~76 % (Fig. 2e, Tables S2 and S4), which is close to the measured COD removal of ~83 %, further confirming the reliability of NMR analysis. The COD from carboxylic acids contributed 85.3 % of the total COD in initial manure wastewater and increased to 90.5 % and 93.9 % after 1-cycle and 3-cycle NH_4^+ recovery (Fig. S4), suggesting that carboxylic acids are more inert against oxidation compared to other metabolites. The volcano plot of all metabolites (Fig. 2f) shows that the concentrations of 11 metabolites significantly decreased with a magnitude of 2-fold or greater after NH_4^+ recovery ($\log_2FC \geqslant 1$ or $\leqslant -1$, purple area). This group of 11 metabolites include amines, amino acids, and metabolite with -OH group, and some carboxylic acids, such as acetate, benzoate,

and pimelate. These results reveal that direct electron transfer drives the oxidation and removal of different organic matter (metabolites) and spontaneous NH_4^+ uptake in manure wastewater.

To gain a deeper understanding on why organic compounds can be oxidized and how they can be removed during spontaneous NH_4^+ uptake, we compared the electrochemical potentials to oxidize various organic compounds[45-49] with the redox potential of the KNiHCF electrode. In 1 M NH_4Cl solution, the redox conversion of the KNiHCF electrode is ~0.68 V vs. standard hydrogen electrode (SHE) (Fig. 3a), which could oxidize some alcohols, amines, and aniline, but is lower than the required oxidization potentials of other metabolites, such as most carboxylic acids.[45] Also, the equivalent charges of COD removal [C(COD, removal)] during NH_4^+ uptake from manure wastewater were larger than the charges passing through the KNiHCF electrode [C(RR)] in electrochemical NH_4^+ recovery (Fig. 3b). This suggests that the direct oxidation of organic compounds only contributed to parts of the observed COD removal.

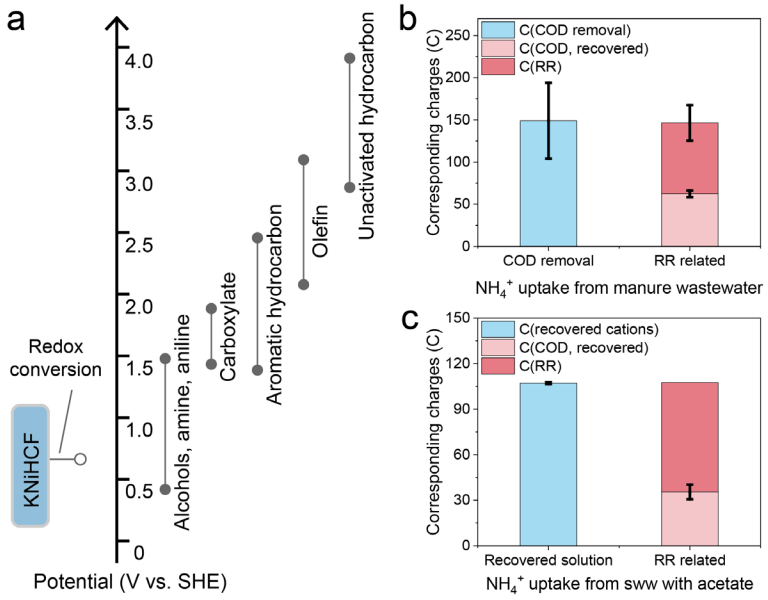

Figure 3. NH_4^+ uptake driven by direct oxidation of organic compounds and adsorption on KNiHCF electrode. (a) Comparison of the redox conversion potential of the KNiHCF electrode and the potentials to oxidize various classes of organic compounds (vs. SHE). (b) Comparison of the equivalent charge of COD removal in manure wastewater [C(COD, removal)] and the RR-related charges in the recovered solution during NH_4^+ uptake from manure wastewater: C(COD, recovered) is the equivalent charge of COD in the recovered solution and C(RR) is the capacity of the KNiHCF electrode. (c) Comparison of the equivalent charge of recovered cations and the RR-

related charges in the recovered solution during NH_4^+ uptake from synthetic wastewater with acetate. C(recovered cations) is the equivalent charge of recovered cations in the recovered solution. Synthetic wastewater with acetate is a mixed solution of 0.35 M NH_4Ac, 0.15 M NH_4Cl, 0.050 M HCOOK, 0.133 M $KHCO_3$ and 0.146 M $NaHCO_3$.

As illustrated in Fig. 1b, a typical direct electron transfer process includes diffusion of reactants from the solution to the surface of the electrode, adsorption of reactants on the electrode, electron transfer between reactants and the electrode, desorption of products, and diffusion of products to the solution.[39] Since adsorption of organic compounds occurs before electron transfer and desorption, we hypothesize that some anions that are adsorbed on the electrode surface or some products that are not easily desorbed can cause cations in manure wastewater to attach to the electrode surface to maintain charge balance (Fig. 1d). To verify this hypothesis, we measured the equivalent charge of COD in the recovered solution [C(COD, recovered)] to reveal the amount of adsorbed organic species during NH_4^+ uptake because such organic species could not be intercalated and released into the recovered solution by the electrode material. We found that C(COD, removal) (149 ± 45 C) was almost equal to the sum of C(COD, recovered) (68 ± 4 C) and C(RR) (84 ± 21 C) in manure wastewater (Fig. 3b and Table S5). In other words, the spontaneous NH_4^+ uptake from manure wastewater included both NH_4^+ intercalation driven by the oxidation of organic matter and NH_4^+ adsorption on the electrode surface. This also explains the observed above 100 % FE for recovered cations in our previous work.[36] We used electron microscopy to characterize the morphology and the porosity of the KNiHCF electrode (Fig. S5). The electrochemical active surface area (ECSA) of the KNiHCF electrode was 24 times higher than the bare substrate (Fig. S6), which suggested that the NH_4^+ adsorption might be related to the surface area of the electrode.

To further confirm the "direct electron transfer and adsorption" mechanism, we conducted electrochemical NH_4^+ uptake in synthetic wastewater with organic anions (see details in Methods). We use synthetic wastewater that contains acetate to represent inert carboxylic acids and formate to represent reactive metabolites. The KNiHCF electrode electrochemically removed NH_4^+ from this synthetic wastewater and released NH_4^+ and adsorbed anions in recovered solutions. The corresponding charges from recovered NH_4^+ cations [C(recovered cations)] were 107. 1 ± 0.5 C, which was close to the sum of C(COD, recovered) (35.5 ± 4.8 C) and C(RR) (72.0 C) (Fig. 3c and

Table S6). Since all ionic species in this synthetic wastewater are monovalent (+1 or -1), such balance between C(recovered cations) and C(COD, recovered) with C(RR) shows that the NH_4^+ uptake from synthetic wastewater with organic anions can come from both NH_4^+ intercalation and adsorption on the electrode surface.

Based on the mechanism of organic matter oxidation elucidated above, the key to improving NH_4^+ uptake efficiency is developing NH_4^+-selective redox materials that can readily oxidize organic compounds. Since the thermodynamic driving force is the potential difference between the redox-active electrode and the organic compounds, redox materials with similar interfaces to KNiHCF but higher oxidation potential should increase the reaction rate. We surveyed PBAs that contain other metal ions, such as Fe^{2+} and Cu^{2+},[50] and studied their cyclic voltammograms (CVs) together with that of KNiHCF (Fig. 4a), in comparison with the oxidation potential of organic matter in manure wastewater (red vertical line). CuHCF should be more potent in oxidizing the organic matter but might be less stable, and FeHCF might be more stable but less effective in oxidizing the organic matter. Based on these, we further designed NH_4^+-selective core-shell electrode materials consisting of core MHCF nanoparticles with different redox potentials and a stable KNiHCF shell (noted as MHCF@KNiHCF, M is Fe or Cu) (Fig. 4a).

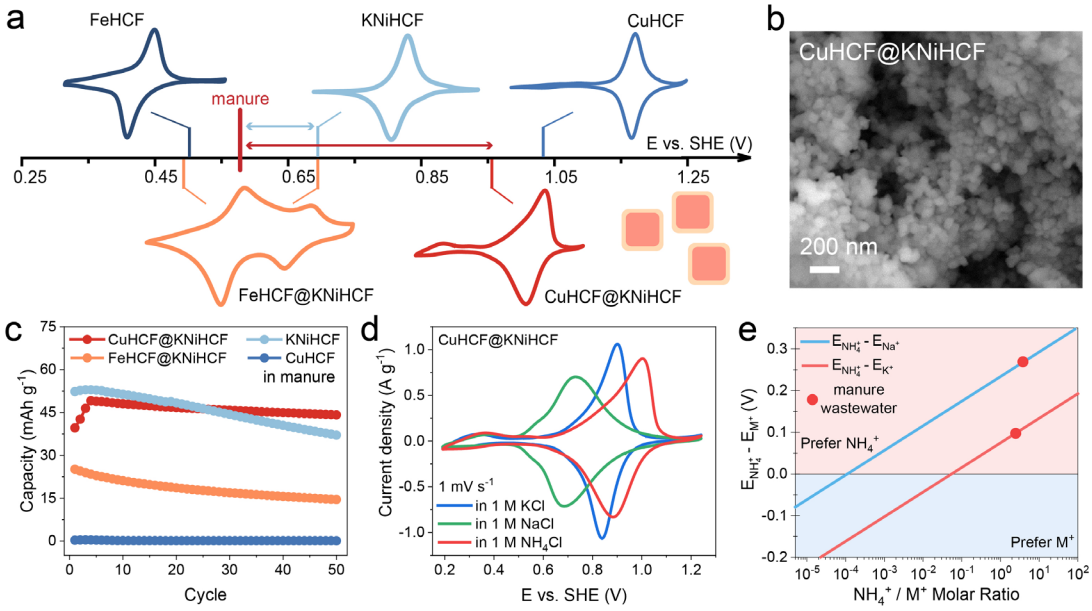

Figure 4. Electrochemical characterizations of Prussian blue analogs (PBAs) with different redox potentials as redox-active electrodes. (a) The electrochemical potential scale showing PBAs with different redox potentials (vertical lines with different colors) in comparison with the

oxidation potential of organic matter in manure wastewater (red vertical line). Zoomed out CVs of these PBAs without vertical axes are shown to highlight the different redox potentials. The boxes with light-red cores and orange shells schematically represent the core-shell PBA nanoparticles. (b) SEM image of the as-synthesized CuHCF@KNiHCF core-shell nanoparticles. (c) Cycling stability of various PBA electrodes in manure wastewater at 2C rate (130 mA g^{-1}). The capacity of FeHCF was nearly zero and not shown here. (d) Cyclic voltammograms of the CuHCF@KNiHCF electrode at 1 mV s^{-1} in solutions of 1 M KCl, 1 M NaCl, and 1 M NH_4Cl. (e) Calculated intercalation potential difference between NH_4^+ and K^+ or Na^+ at different molar ratios of NH_4^+/K^+ or Na^+. The red dots show the actual NH_4^+/K^+ or Na^+ concentration ratios in the manure wastewater used in this study.

We synthesized different core-shell PBA nanoparticles via a two-step process,[51, 52] including synthesis of core MHCF nanoparticles and forming the KNiHCF shell on the surface of these core nanoparticles (Methods and Fig. S7). The diameter of the as-synthesized core-shell PBA nanoparticles was ~50 nm (Fig. 4b and Fig. S8), similar to the core nanoparticles, indicating that the formed shells were thin. The Powder X-ray diffraction (PXRD) patterns of these nanoparticles matched well with the standard pattern of the cubic phase of Prussian blue (JCPDS No. 52-1907) (Fig. S9). The chemical formulas of these materials were determined using thermal gravimetric analysis (TGA) and inductively coupled plasma optical emission spectroscopy (ICP-OES) (Table S7), e.g., CuHCF@KNiHCF ($K_{0.1}Cu_{0.77}Ni_{0.64}[Fe(CN)_6] \cdot 4.8\ H_2O$) and FeHCF@KNiHCF ($K_{0.17}Ni_{0.75}Fe_{0.75}[Fe(CN)_6] \cdot 3.7\ H_2O$).

We evaluated the redox potentials of these PBA electrodes in 1 M NH_4Cl solution and their cycling stability in manure wastewater. Cyclic voltammograms (CV) of these electrodes showed that the redox potentials from high to low were CuHCF, CuHCF@KNiHCF, KNiHCF, FeHCF@KNiHCF, and FeHCF (Fig. 4a and Fig. S10). Compared to KNiHCF, after introducing the high-potential CuHCF core, the thermodynamic driving force of CuHCF@KNiHCF for oxidation of organic matter could increase from 0.10 V to 0. 35 V. Considering the similar interface and a higher redox potential from the core-shell design, CuHCF@KNiHCF should result in more effective oxidation of organic species and faster NH_4^+ recovery from manure wastewater than KNiHCF. Pure CuHCF and FeHCF were electrochemically unstable in manure wastewater based on their CV profiles (Fig. S11a) and galvanostatic charge-discharge (GCD) tests at a 2 C rate (Fig.

4c). Here, the 1 C rate is 65 mA g^{-1} based on the theoretical capacity. However, core-shell CuHCF@KNiHCF and FeHCF@KNiHCF electrodes with KNiHCF shells showed improved cycling stability (Fig. 4c and Fig. S11b). Specifically, the CuHCF@KNiHCF electrode exhibited better capacity retention (44 mAh g^{-1} at the 50th cycle, ~90 % over 50 cycles) than the KNiHCF electrode (37 mAh g^{-1} at the 50th cycle, ~70 % over 50 cycles). We then further optimized the shell thickness of core-shell CuHCF@KNiHCF by varying the shell reaction time (see Methods and Table S7) and all core-shell CuHCF@KNiHCF samples exhibited similar particle sizes and diffraction peaks (Fig. S12). The CuHCF@KNiHCF electrode with a thicker KNiHCF shell showed better cycling stability but reduced capacity, and the CuHCF@KNiHCF electrode with a thinner shell was unstable in manure wastewater (Fig. S13). Hence, proper thickness of the KNiHCF shell is essential to achieve excellent stability and good capacity.

Cation intercalation selectivity of the CuHCF@KNiHCF electrode was studied in 1 M KCl, 1 M NaCl, and 1 M NH_4Cl solutions. The CV profiles showed reversible interaction of NH_4^+, K^+, and Na^+ at 0.944 V, 0.872 V, and 0.708 V vs. SHE (Fig. 4d and Table S8), respectively, which were at higher potentials than those of KNiHCF.[36] Calculated potential differences of cation intercalation at different molar ratios of NH_4^+/Na^+ reveal that NH_4^+ intercalation is thermodynamically favorable when NH_4^+/Na^+ ratio is above 3×10^{-5} (Fig. 4e and Note S2). The CuHCF@KNiHCF electrode shows higher potential differences at the actual NH_4^+/ Na^+ concentration ratios in manure wastewater than the KNiHCF electrode (Table S8). These results suggest that the CuHCF@KNiHCF electrode can selectively recover NH_4^+ ions and may have better ion selectivity than the KNiHCF electrode.

Finally, we employed the optimized CuHCF@KNiHCF electrode in the electrochemical NH_4^+ recovery from manure wastewater, investigated its performance and optimized the operation conditions. Based on our previous report, the Q_{NH4+}/Q_{RR} ratios influenced the average NH_4^+ removal rate, where Q_{NH4+} is the minimal charge to recover NH_4^+ in manure wastewater, and Q_{RR} is the capacity of the redox electrode.[36] Two parallel NH_4^+ recovery processes (run 1 and run 2, in which the same redox-active electrode was evaluated in two batches of manure wastewater) at $Q_{NH4+}/Q_{RR} = 1$ showed the NH_4^+ removal of ~77 % and COD removal of ~38 % (Fig. S14a and S12b). There was nearly no NH_4^+ loss in the NH_4^+ uptake process (Fig. S14c-e). The Coulombic efficiency related to COD removal, defined as the ratio of the charges passing through the RR (C_{RR})

to the charges needed for COD removal (C_{COD}), was ~ 30 % (Fig. S14d). The NH_4^+ / Na^+ (K^+) selectivity was 6~7 (1.4~1.6) (Fig. S14f). These results were similar to those achieved in NH_4^+ uptake using the KNiHCF electrode. To improve NH_4^+ removal in manure wastewater, we used a CuHCF@KNiHCF electrode with a higher mass loading and conducted NH_4^+ recovery processes at Q_{NH4+}/Q_{RR} = 0.77. The NH_4^+ removal was ~80 % with a reduced NH_4^+ concentration of ~400 mM in manure wastewater (Fig. 5a). The CE related to COD removal was also ~30 % for each run (Fig. S15a). COD removal increased to 41 % compared to 38% at Q_{NH4+}/Q_{RR} = 1 (Fig. S15b). NH_4^+, K^+, and Na^+ ions were balanced without apparent loss during NH_4^+ uptake (Fig. S15c and 15d). On average, after just one-cycle recovery, 80 % NH_4^+ ions were recovered (and 20 % NH_4^+ were left in manure wastewater), much higher than the 68 % NH_4^+ recovery using the KNiHCF electrode at similar conditions.

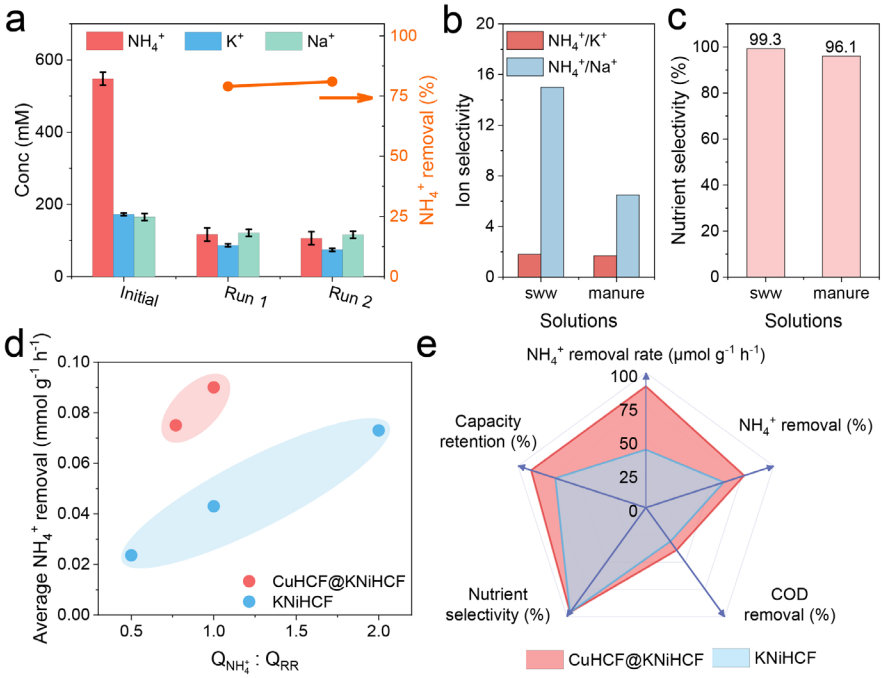

Figure 5. Electrochemical NH_4^+ recovery from manure wastewater using the CuHCF@KNiHCF electrode. (a) Concentration changes and NH_4^+ removal over the two recovery runs from manure wastewater. (b) Ion selectivity (NH_4^+/Na^+ and NH_4^+/K^+) of NH_4^+ recovery in manure wastewater (manure) and synthetic wastewater (sww). Synthetic wastewater is a mixed solution of 0.50 M NH_4Cl, 0.183 M $KHCO_3$, and 0.146 M $NaHCO_3$. (c) Nutrient selectivity in synthetic wastewater and manure wastewater. Nutrient selectivity is defined as the concentration of NH_4^+ and K^+ in the recovered solution to the total concentration of released

cations. (d) NH_4^+ removal rate using CuHCF@KNiHCF and KNiHCF electrodes at different operation conditions of Q_{NH4+}/Q_{RR} ratios. Q_{NH4+} is the minimal charge to recover NH_4^+ in manure wastewater and Q_{RR} is the capacity of the redox-active electrode. (e) Comparison of the various NH_4^+ recovery performance metrics using the CuHCF@KNiHCF electrode with the previously reported KNiHCF electrode in a multivariate radar chart.

The ion selectivity of the CuHCF@KNiHCF electrode in manure wastewater was lower than that in synthetic wastewater (Fig. 5b and Fig. S13f). Especially, the NH_4^+/Na^+ selectivity was 7 in manure wastewater and 15 in synthetic wastewater. This reduced ion selectivity in manure wastewater was in line with the more complex NH_4^+ uptake mechanisms (intercalation plus absorption) discussed above -- the less selective ion adsorption on the electrode surface would reduce the overall ion selectivity. The overall nutrient selectivity in manure wastewater (96.1 %) was slightly lower than the 99.3 % observed in synthetic wastewater (Fig. 5c). Here, nutrient selectivity is defined as the concentration of NH_4^+ and K^+ in the recovered solution to the total concentration of released cations. Importantly, the CuHCF@KNiHCF electrode, with an improved thermodynamic driving force, achieved significantly increased average NH_4^+ removal rate (~0.9 mmol g^{-1} h^{-1}), twice as much as the that by KNiHCF electrode under the same operation conditions (Fig. 5d and Table S9). NMR analysis of manure wastewater after 1-cycle recovery using CuHCF@KNiHCF also revealed that more metabolites were removed than KNiHCF (Table S10). The calculated COD removal was also consistent with the measured COD removal (Tables S11 and S12), indicating that CuHCF@KNiHCF could oxidize more organic compounds than KNiHCF. The CuHCF@KNiHCF, designed based on the elucidated oxidation and NH_4^+ uptake mechanisms, could deliver improved performance in all five critical metrics for NH_4^+-selective redox materials compared to previously reported KNiHCF (Fig. 5e).

Conclusion

In summary, we studied the mechanisms for the spontaneous oxidation of organic matter and NH_4^+ uptake from manure wastewater on redox-active KNiHCF material and further developed NH_4^+-selective core-shell PBA electrode material that showed enhanced stability and NH_4^+ uptake. Pasteurization or freezing treatment of manure wastewater allowed us to confirm that the direct electron transfer from organic matter to the KNiHCF electrode is the dominant process and drives the spontaneous NH_4^+ uptake. NMR analysis revealed that many different types

of metabolites, including amines, amino acids and more inert carboxylic acids, were removed by the KNiHCF electrode. Furthermore, we found that the NH_4^+ uptake from manure wastewater involved both selective NH_4^+ intercalation into the KNiHCF electrode and the cation adsorption on the electrode surface to maintain the charge balance from absorbed organic anions. This "direct electron transfer + adsorption" mechanism was confirmed in synthetic wastewater with organic anions. Guided by the elucidated mechanisms, we further developed NH_4^+-selective core-shell electrode material with a stable KNiHCF shell and a high-potential CuHCF core, which can increase thermodynamic driving force for the oxidation of organic compounds. Such a core-shell CuHCF@KNiHCF achieved improved stability in manure wastewater and nearly twice the NH_4^+ removal rate compared to previously reported KNiHCF. These results provide more fundamental understanding of spontaneous oxidation of organic compounds and selective ion uptake by redox-active materials and can guide the future design of effective redox materials for resource recovery and environmental applications.

ASSOCIATE CONTENT

Corresponding Author

Correspondence and requests for materials should be addressed to S. J. (jin@chem.wisc.edu). ORCID: 0000-0001-8693-7010.

Acknowledgements

This research is supported by the National Science Foundation (NSF, CBET-2219089). The authors acknowledge the facilities and instrumentation at the UW-Madison Wisconsin Centers for Nanoscale Technology (wcnt.wisc.edu), partially supported by the NSF through the University of Wisconsin Materials Research Science and Engineering Center (no. DMR-2309000). We thank J. Lazarcik for help with the access to the IC and ICP–OES instruments supported by the Water Science and Engineering Laboratory at UW-Madison. We thank P. R. Pinheiro for help with the access to the licensed Chenomx software.

Additional information

Supporting information is available for this paper in the online version of the paper. Materials and methods, material characterizations, additional notes on COD calculations, additional tables and figures on NMR analysis and ammonium recovery results.

Ethics declarations

Competing interests

The authors declare no competing interests.

References

(1) Liang, G.; Mo, F.; Ji, X.; Zhi, C. Non-metallic charge carriers for aqueous batteries. *Nat. Rev. Mater.* **2021**, *6* (2), 109-123. DOI: 10.1038/s41578-020-00241-4.

(2) Goodenough, J. B. Evolution of Strategies for Modern Rechargeable Batteries. *Acc. Chem. Res.* **2013**, *46* (5), 1053-1061. DOI: 10.1021/ar2002705.

(3) Konarov, A.; Voronina, N.; Jo, J. H.; Bakenov, Z.; Sun, Y.-K.; Myung, S.-T. Present and Future Perspective on Electrode Materials for Rechargeable Zinc-Ion Batteries. *ACS Energy Lett.* **2018**, *3* (10), 2620-2640. DOI: 10.1021/acsenergylett.8b01552.

(4) Qiu, T.; Liang, Z.; Guo, W.; Tabassum, H.; Gao, S.; Zou, R. Metal–Organic Framework-Based Materials for Energy Conversion and Storage. *ACS Energy Lett.* **2020**, *5* (2), 520-532. DOI: 10.1021/acsenergylett.9b02625.

(5) Whittingham, M. S. Lithium Batteries and Cathode Materials. *Chem. Rev.* **2004**, *104* (10), 4271-4302. DOI: 10.1021/cr020731c.

(6) Tamirat, A. G.; Guan, X.; Liu, J.; Luo, J.; Xia, Y. Redox mediators as charge agents for changing electrochemical reactions. *Chemical Society Reviews* **2020**, *49* (20), 7454-7478. DOI: 10.1039/d0cs00489h.

(7) Michael, K. H.; Su, Z.-M.; Wang, R.; Sheng, H.; Li, W.; Wang, F.; Stahl, S. S.; Jin, S. Pairing of Aqueous and Nonaqueous Electrosynthetic Reactions Enabled by a Redox Reservoir Electrode. *J Am Chem Soc* **2022**, *144* (49), 22641-22650. DOI: 10.1021/jacs.2c09632.

(8) Wang, F.; Li, W.; Wang, R.; Guo, T.; Sheng, H.; Fu, H.-C.; Stahl, S. S.; Jin, S. Modular Electrochemical Synthesis Using a Redox Reservoir Paired with Independent Half-Reactions. *Joule* **2021**, *5* (1), 149-165. DOI: 10.1016/j.joule.2020.11.011.

(9) Wang, R.; Sheng, H.; Wang, F.; Li, W.; Roberts, D. S.; Jin, S. Sustainable Coproduction of Two Disinfectants via Hydroxide-Balanced Modular Electrochemical Synthesis Using a Redox Reservoir. *Acs Central Sci* **2021**, *7* (12), 2083-2091. DOI: 10.1021/acscentsci.1c01157.

(10) Chen, L.; Dong, X.; Wang, Y.; Xia, Y. Separating hydrogen and oxygen evolution in alkaline water electrolysis using nickel hydroxide. *Nat Commun* **2016**, *7* (1), 11741. DOI: 10.1038/ncomms11741.

(11) Hou, M.; Chen, L.; Guo, Z.; Dong, X.; Wang, Y.; Xia, Y. A clean and membrane-free chlor-alkali process with decoupled Cl2 and H2/NaOH production. *Nat Commun* **2018**, *9* (1), 438. DOI: 10.1038/s41467-018-02877-x.

(12) Dotan, H.; Landman, A.; Sheehan, S. W.; Malviya, K. D.; Shter, G. E.; Grave, D. A.; Arzi, Z.; Yehudai, N.; Halabi, M.; Gal, N.; et al. Decoupled hydrogen and oxygen evolution by a two-step electrochemical–chemical cycle for efficient overall water splitting. *Nat Energy* **2019**, *4* (9), 786-795. DOI: 10.1038/s41560-019-0462-7.

(13) Landman, A.; Dotan, H.; Shter, G. E.; Wullenkord, M.; Houaijia, A.; Maljusch, A.; Grader, G. S.; Rothschild, A. Photoelectrochemical water splitting in separate oxygen and hydrogen cells. *Nature Materials* **2017**, *16* (6), 646-651. DOI: 10.1038/nmat4876.

(14) Wang, R.; Ma, J.; Sheng, H.; Zavala, V. M.; Jin, S. Exploiting different electricity markets via highly rate-mismatched modular electrochemical synthesis. *Nat Energy* **2024**. DOI: 10.1038/s41560-024-01578-8.

(15) Heiskanen, S. K.; Kim, J.; Lucht, B. L. Generation and Evolution of the Solid Electrolyte Interphase of Lithium-Ion Batteries. *Joule* **2019**, *3* (10), 2322-2333. DOI: 10.1016/j.joule.2019.08.018.

(16) Peled, E.; Menkin, S. Review—SEI: Past, Present and Future. *Journal of The Electrochemical Society* **2017**, *164* (7), A1703-A1719. DOI: 10.1149/2.1441707jes.

(17) George, M. V.; Balachandran, K. S. Nickel-peroxide oxidation of organic compounds. *Chem. Rev.* **1975**, *75* (4), 491-519. DOI: 10.1021/cr60296a004.

(18) Evans, D. L.; Minster, D. K.; Jordis, U.; Hecht, S. M.; Mazzu, A. L.; Meyers, A. I. Nickel peroxide dehydrogenation of oxygen-, sulfur-, and nitrogen-containing heterocycles. *J. Org. Chem.* **1979**, *44* (4), 497-501. DOI: 10.1021/jo01318a005.

(19) Schäfer, H. J.; Schneider, R. Oxidation of partially protected carbohydrates at the nickel hydroxide electrode. *Tetrahedron* **1991**, *47* (4-5), 715-724. DOI: 10.1016/s0040-4020(01)87061-7.

(20) Easton, C. J.; Eichinger, S. K.; Pitt, M. J. Nickel peroxide as a glycine-selective chemical model of peptidylglycine α-amidating monooxygenase. *J. Chem. Soc., Chem. Commun.* **1992**, *0* (18), 1295-1296. DOI: 10.1039/c39920001295.

(21) Remucal, C. K.; Ginder-Vogel, M. A critical review of the reactivity of manganese oxides with organic contaminants. *Environ. Sci.: Process. Impacts* **2014**, *16* (6), 1247-1266. DOI: 10.1039/c3em00703k.

(22) Sunda, W. G.; Kieber, D. J. Oxidation of humic substances by manganese oxides yields low-molecular-weight organic substrates. *Nature* **1994**, *367* (6458), 62-64. DOI: 10.1038/367062a0.

(23) Stone, A. T.; Morgan, J. J. Reduction and dissolution of manganese(III) and manganese(IV) oxides by organics: 2. Survey of the reactivity of organics. *Environ. Sci. Technol.* **1984**, *18* (8), 617-624. DOI: 10.1021/es00126a010.

(24) Stone, A. T.; Morgan, J. J. Reduction and dissolution of manganese(III) and manganese(IV) oxides by organics. 1. Reaction with hydroquinone. *Environ. Sci. Technol.* **1984**, *18* (6), 450-456. DOI: 10.1021/es00124a011.

(25) Stone, A. T. Reductive Dissolution of Manganese(III/Iv) Oxides by Substituted Phenols. *Environ. Sci. Technol.* **1987**, *21* (10), 979-988. DOI: 10.1021/es50001a011.

(26) Li, H.; Santos, F.; Butler, K.; Herndon, E. A Critical Review on the Multiple Roles of Manganese in Stabilizing and Destabilizing Soil Organic Matter. *Environ. Sci. Technol.* **2021**, *55* (18), 12136-12152. DOI: 10.1021/acs.est.1c00299.

(27) Trainer, E. L.; Ginder-Vogel, M.; Remucal, C. K. Selective Reactivity and Oxidation of Dissolved Organic Matter by Manganese Oxides. *Environ. Sci. Technol.* **2021**, *55* (17), 12084-12094. DOI: 10.1021/acs.est.1c03972.

(28) Noh, H.; Mayer, J. M. Medium-independent hydrogen atom binding isotherms of nickel oxide electrodes. *Chem* **2022**, *8* (12), 3324-3345. DOI: 10.1016/j.chempr.2022.08.018.

(29) Bender, M. T.; Lam, Y. C.; Hammes-Schiffer, S.; Choi, K.-S. Unraveling Two Pathways for Electrochemical Alcohol and Aldehyde Oxidation on NiOOH. *J Am Chem Soc* **2020**, *142* (51), 21538-21547. DOI: 10.1021/jacs.0c10924.

(30) Zuo, K.; Garcia-Segura, S.; Cerrón-Calle, G. A.; Chen, F.-Y.; Tian, X.; Wang, X.; Huang, X.; Wang, H.; Alvarez, P. J. J.; Lou, J.; et al. Electrified water treatment: fundamentals and roles of electrode materials. *Nat. Rev. Mater.* **2023**, *8* (7), 472-490. DOI: 10.1038/s41578-023-00564-y.

(31) Kim, T.; Gorski, C. A.; Logan, B. E. Ammonium Removal from Domestic Wastewater Using Selective Battery Electrodes. *Environ Sci Tech Let* **2018**, *5* (9), 578-583. DOI: 10.1021/acs.estlett.8b00334.

(32) Liu, C.; Li, Y.; Lin, D.; Hsu, P.-C.; Liu, B.; Yan, G.; Wu, T.; Cui, Y.; Chu, S. Lithium Extraction from Seawater through Pulsed Electrochemical Intercalation. *Joule* **2020**, *4* (7), 1459-1469. DOI: 10.1016/j.joule.2020.05.017.

(33) Yan, G.; Wang, M.; Hill, G. T.; Zou, S.; Liu, C. Defining the challenges of Li extraction with olivine host: The roles of competitor and spectator ions. *Proc National Acad Sci* **2022**, *119* (31), e2200751119. DOI: 10.1073/pnas.2200751119.

(34) Son, M.; Kolvek, E.; Kim, T.; Yang, W.; Vrouwenvelder, J. S.; Gorski, C. A.; Logan, B. E. Stepwise ammonium enrichment using selective battery electrodes. *Environmental Science: Water Research & Technology* **2020**, *6* (6), 1649-1657, 10.1039/D0EW00010H. DOI: 10.1039/D0EW00010H.

(35) Chen, W.; Akinyemi, P.; Kim, T. Selective Separation of Ammonium from Wastewater Using Ion Conducting Channels of a Prussian Blue Analogue. *Environ Sci Tech Let* **2024**, *11* (3), 280-286. DOI: 10.1021/acs.estlett.3c00932.

(36) Wang, R.; Yang, K.; Wong, C.; Aguirre-Villegas, H.; Larson, R.; Brushett, F.; Qin, M.; Jin, S. Electrochemical ammonia recovery and co-production of chemicals from manure wastewater. *Nature Sustainability* **2024**, *7* (2), 179-190. DOI: 10.1038/s41893-023-01252-z.

(37) Zhu, C.; Li, C.; Wang, Y.; Laghi, L. Characterization of Yak Common Biofluids Metabolome by Means of Proton Nuclear Magnetic Resonance Spectroscopy. *Metabolites* **2019**, *9* (3), 41. DOI: 10.3390/metabo9030041.

(38) Kim, H. S.; Kim, E. T.; Eom, J. S.; Choi, Y. Y.; Lee, S. J.; Lee, S. S.; Chung, C. D.; Lee, S. S. Exploration of metabolite profiles in the biofluids of dairy cows by proton nuclear magnetic resonance analysis. *Plos One* **2021**, *16* (1), e0246290. DOI: 10.1371/journal.pone.0246290.

(39) Balzani, V.; Piotrowiak, P.; Rodgers, M.; Mattay, J.; Astruc, D. *Electron transfer in chemistry*; Wiley-VCh Weinheim, 2001.

(40) Hernandez, M. E.; Newman, D. K. Extracellular electron transfer. *Cell Mol Life Sci Cmls* **2001**, *58* (11), 1562-1571. DOI: 10.1007/pl00000796.

(41) Kumar, A.; Hsu, L. H.-H.; Kavanagh, P.; Barrière, F.; Lens, P. N. L.; Lapinsonnière, L.; V, J. H. L.; Schröder, U.; Jiang, X.; Leech, D. The ins and outs of microorganism–electrode electron transfer reactions. *Nat. Rev. Chem.* **2017**, *1* (3), 0024. DOI: 10.1038/s41570-017-0024.

(42) Leung, P.; Shah, A. A.; Sanz, L.; Flox, C.; Morante, J. R.; Xu, Q.; Mohamed, M. R.; León, C. P. d.; Walsh, F. C. Recent developments in organic redox flow batteries: A critical review. *J Power Sources* **2017**, *360*, 243-283. DOI: 10.1016/j.jpowsour.2017.05.057.

(43) Winsberg, J.; Hagemann, T.; Janoschka, T.; Hager, M. D.; Schubert, U. S. Redox-Flow Batteries: From Metals to Organic Redox-Active Materials. *Angew. Chem. Int. Ed.* **2017**, *56* (3), 686-711. DOI: 10.1002/anie.201604925.

(44) Luo, J.; Hu, B.; Hu, M.; Zhao, Y.; Liu, T. L. Status and Prospects of Organic Redox Flow Batteries toward Sustainable Energy Storage. *ACS Energy Lett.* **2019**, *4* (9), 2220-2240. DOI: 10.1021/acsenergylett.9b01332.

(45) Luca, O. R.; Gustafson, J. L.; Maddox, S. M.; Fenwick, A. Q.; Smith, D. C. Catalysis by electrons and holes: formal potential scales and preparative organic electrochemistry. *Org. Chem. Front.* **2015**, *2* (7), 823-848. DOI: 10.1039/c5qo00075k.

(46) Radjenovic, J.; Duinslaeger, N.; Avval, S. S.; Chaplin, B. P. Facing the Challenge of Poly- and Perfluoroalkyl Substances in Water: Is Electrochemical Oxidation the Answer? *Environ. Sci. Technol.* **2020**, *54* (23), 14815-14829. DOI: 10.1021/acs.est.0c06212.

(47) Reid, L. M.; Li, T.; Cao, Y.; Berlinguette, C. P. Organic chemistry at anodes and photoanodes. *Sustain. Energy Fuels* **2018**, *2* (9), 1905-1927. DOI: 10.1039/c8se00175h.

(48) Roth, H.; Romero, N.; Nicewicz, D. Experimental and Calculated Electrochemical Potentials of Common Organic Molecules for Applications to Single-Electron Redox Chemistry. *Synlett* **2015**, *27* (05), 714-723. DOI: 10.1055/s-0035-1561297.

(49) Chipoco Haro, D. A.; Barrera, L.; Iriawan, H.; Herzog, A.; Tian, N.; Medford, A. J.; Shao-Horn, Y.; Alamgir, F. M.; Hatzell, M. C. Electrocatalysts for Inorganic and Organic Waste Nitrogen Conversion. *ACS Catalysis* **2024**, *14* (13), 9752-9775. DOI: 10.1021/acscatal.4c01398.

(50) Hurlbutt, K.; Wheeler, S.; Capone, I.; Pasta, M. Prussian Blue Analogs as Battery Materials. *Joule* **2018**, *2* (10), 1950-1960. DOI: 10.1016/j.joule.2018.07.017.

(51) Asakura, D.; Li, C. H.; Mizuno, Y.; Okubo, M.; Zhou, H.; Talham, D. R. Bimetallic Cyanide-Bridged Coordination Polymers as Lithium Ion Cathode Materials: Core@Shell Nanoparticles with Enhanced Cyclability. *J Am Chem Soc* **2013**, *135* (7), 2793-2799. DOI: 10.1021/ja312160v.

(52) Wan, M.; Tang, Y.; Wang, L.; Xiang, X.; Li, X.; Chen, K.; Xue, L.; Zhang, W.; Huang, Y. Core-shell hexacyanoferrate for superior Na-ion batteries. *J Power Sources* **2016**, *329*, 290-296. DOI: 10.1016/j.jpowsour.2016.08.059.

TOC graph

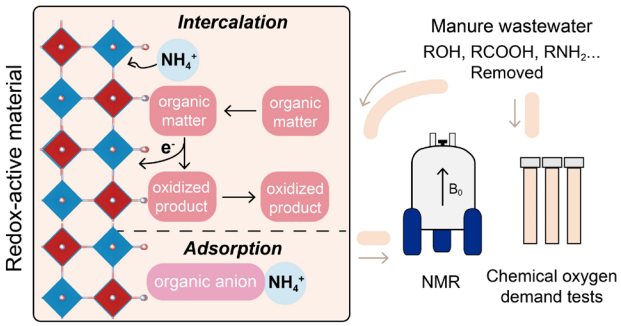
Intercalation
Redox-active material
NH4+
organic matter
organic matter
e-
oxidized product
oxidized product
Adsorption
organic anion
NH4+
Manure wastewater
ROH, RCOOH, RNH2...
Removed
B0
NMR
Chemical oxygen demand tests